ResearchGate

See discussions, stats, and author profiles for this publication at: https://www.researchgate.net/publication/5675038

Isotropic Chemical Shifts in Magic-Angle Spinning NMR Spectra of Proteins

ARTICLE *in* PHYSICAL CHEMISTRY CHEMICAL PHYSICS · FEBRUARY 2008

Impact Factor: 4.49 · DOI: 10.1039/b710736f · Source: PubMed

CITATIONS
6

READS
34

3 AUTHORS, INCLUDING:

Benjamin J Wylie
Texas Tech University
25 PUBLICATIONS **949** CITATIONS
SEE PROFILE

Chad Michael Rienstra
University of Illinois, Urbana-Champaign
109 PUBLICATIONS **5,604** CITATIONS
SEE PROFILE

Available from: Chad Michael Rienstra
Retrieved on: 24 January 2016

Isotropic chemical shifts in magic-angle spinning NMR spectra of proteins†

Benjamin J. Wylie,[a] Lindsay J. Sperling[a] and Chad M. Rienstra*[abc]

Received 13th July 2007, Accepted 19th October 2007
First published as an Advance Article on the web 5th November 2007
DOI: 10.1039/b710736f

Here we examine the effect of magic-angle spinning (MAS) rate upon lineshape and observed peak position for backbone carbonyl (C′) peaks in NMR spectra of uniformly-^{13}C,^{15}N-labeled (U–^{13}C,^{15}N) solid proteins. 2D N–C' spectra of U–^{13}C,^{15}N microcrystalline protein GB1 were acquired at six MAS rates, and the site-resolved C′ lineshapes were analyzed by numerical simulations and comparison to spectra from a sparsely labeled sample (derived from 1,3-^{13}C–glycerol). Spectra of the U–^{13}C,^{15}N sample demonstrate large variations in the signal-to-noise ratio and peak positions, which are absent in spectra of the sparsely labeled sample, in which most ^{13}C′ sites do not possess a directly bonded ^{13}CA. These effects therefore are a consequence of rotational resonance, which is a well-known phenomenon. Yet the magnitude of this effect pertaining to chemical shift assignment has not previously been examined. To quantify these effects in high-resolution protein spectra, we performed exact numerical two- and four-spin simulations of the C′ lineshapes, which reproduced the experimentally observed features. Observed peak positions differ from the isotropic shift by up to 1.0 ppm, even for MAS rates relatively far (a few ppm) from rotational resonance. Although under these circumstances the correct isotropic chemical shift values may be determined through simulation, systematic errors are minimized when the MAS rate is equivalent to ~85 ppm for ^{13}C. This moderate MAS condition simplifies spectral assignment and enables data sets from different labeling patterns and spinning rates to be used most efficiently for structure determination.

1. Introduction

Accurate structures of globular, membrane and fibrous proteins are fundamental for modern biomolecular research. However, many macromolecules have low solubility and poor crystallinity and are not, therefore, suitable for either solution NMR or crystallography. Solid-state nuclear magnetic resonance (SSNMR) is a rapidly emerging technique for determining global structure, function and dynamics of such biomolecules.[1–10] Many modern SSNMR structure determination techniques require a set of uniquely assigned chemical shifts, which alone constrain structure,[11] and also serve as the basis for site-resolved measurements of other molecular properties. In most assignment protocols, chemical shift correlations are identified and assigned using data from uniformly-^{13}C,^{15}N-labeled (U–^{13}C,^{15}N) samples.[12–19] This information is complemented with dipolar correlation experiments, from which cross peak intensities as a function of mixing time reveal internuclear distances; such experiments for distance determinations have so far been performed primarily with samples prepared with sparse isotopic labels.[3,9,20,21]

The logic of such a protocol relies upon the critical assumption that peak positions for most ^{13}C resonances will not change significantly in samples with sparse labels, relative to the U–^{13}C,^{15}N samples. If, however, peak positions were to change greatly upon modification of the isotopic labeling pattern, spectral assignment may become significantly less efficient and/or accurate, compromising convergence of structure calculations especially in automated protocols. The degree to which such errors might propagate depends upon the amplitude of the chemical shift perturbations observed under typical experimental conditions.

In protein spectra the carbonyl (C′) region is critical for establishing unique backbone connectivities in assignment protocols, but is also especially susceptible to residual dipolar broadening or perturbations in the peak positions as a function of magic-angle spinning (MAS) rate. The choice of optimal MAS rate is non-trivial. With standard size rotors for protein MAS NMR (2.5 to 4.0 mm) at moderate-to-high field (500 to 800 MHz), the optimal MAS rate falls between the $n = 1$ and $n = 2$ rotational resonance (R^2) conditions;[24–29] *i.e.*, where the spinning rate is less than the C′–CA chemical shift difference, which we define as a "moderate" spinning rate for subsequent discussion. ("Slow" is a spinning rate much less than the chemical shift difference, and "fast" is much greater.)

[a] *Department of Chemistry, University of Illinois at Urbana-Champaign, 600 South Mathews Avenue, Urbana, 61801, Illinois. E-mail: rienstra@scs.uiuc.edu*
[b] *Department of Biochemistry, University of Illinois at Urbana-Champaign, Urbana, 600 South Mathews Avenue, Illinois 61801. E-mail: rienstra@scs.uiuc.edu*
[c] *Center for Biophysics and Computational Biology, University of Illinois at Urbana-Champaign, Urbana, 600 South Mathews Avenue, Illinois 61801. E-mail: rienstra@scs.uiuc.edu*

† Electronic supplementary information (ESI) available: Additional experimental details and simulations. See DOI: 10.1039/b710736f

This journal is © the Owner Societies 2008

For example, at 500 MHz a commonly employed spinning rate in the moderate regime is approximately 11 kHz; in relative terms, this ratio of spinning rate to magnetic field strength has been used now in several SSNMR protein assignment studies.[14,18,22] However, recent studies have also utilized sample spinning at the "weak coupling limit,"[23] which are very close to C′–CA R^2 conditions, corresponding to ~7.8 kHz (for $n = 2$) or 15.6 kHz ($n = 1$) on a 500 MHz spectrometer. Spectra acquired under these conditions risk significant line broadening or peak shifts associated with the residual dipolar coupling near R^2.

The sensitivity of the carbonyl region to these effects, even when avoiding exact R^2 conditions, is a consequence of large chemical shift anisotropy (CSA),[24–29] as first predicted by Maricq and Waugh,[30] and later analyzed in detail by several others.[24–26,31–38] Owing to the dynamically homogeneous Hamiltonian,[30] as the CSA magnitude of one ^{13}C site within a dipole-coupled spin system exceeds the MAS rate (as in the moderate MAS regime), significant lineshape distortions are observed away from exact R^2 conditions.[24–26,31] Therefore the isotropic doublet arising from the scalar C′–CA coupling (~55 Hz) is commonly distorted. The asymmetric ^{13}C lineshapes might also exhibit fine structure and asymmetries from other sources such as ^{1}H and ^{15}N decoupling, but homonuclear near-R^2 effects and CSA-dipole cross correlation are dominant.[24,25,31–38] Such lineshape effects have been utilized to determine internuclear distances in ^{13}C labeled compounds, where chemical shift assignments did not depend critically upon exact resonance frequencies.[27–29]

To our knowledge, there has not yet been a systematic study of the impact of MAS rate upon the sensitivity, resolution and observed peak positions of ^{13}C signals in protein spectra in the regime of moderate MAS rates, ~7 to 15 kHz. This is the experimental regime that has been utilized so far for the majority of SSNMR studies of U–^{13}C,^{15}N-labeled proteins. Here we examine these effects quantitatively by acquiring ^{15}N–^{13}C 2D correlation spectra over a range of spinning rates, analyzing the lineshapes with numerical simulations, and reporting the changes in observed peak position and signal-to-noise ratio (SNR) over a range of conditions. Understanding these effects is both technically important to ensure optimal spectroscopic performance, and also contributes fundamentally to understanding chemical shifts.

2. Results and discussion

2.1 Effect of MAS rate upon NC′ correlation spectra

Two-dimensional heteronuclear correlation spectra of the microcrystalline protein GB1 were acquired at 500 MHz ^{1}H frequency and several MAS rates between ~8.0 and 13.5 kHz (Fig. 1). To enable quantitative lineshape fitting, the spectra were digitized to maximum evolution (^{15}N) and acquisition (^{13}C) times of ~40 ms. (Although the high thermostability of GB1 permits such high-power ^{1}H decoupling, similar parameters could be achieved for less thermostable samples using low electric-field resonator probes).[39] Under these experimental conditions, the observed average T_2 values are ~20 ms for the ^{13}C′ region and ~40 ms for amide ^{15}N region. Two sets of

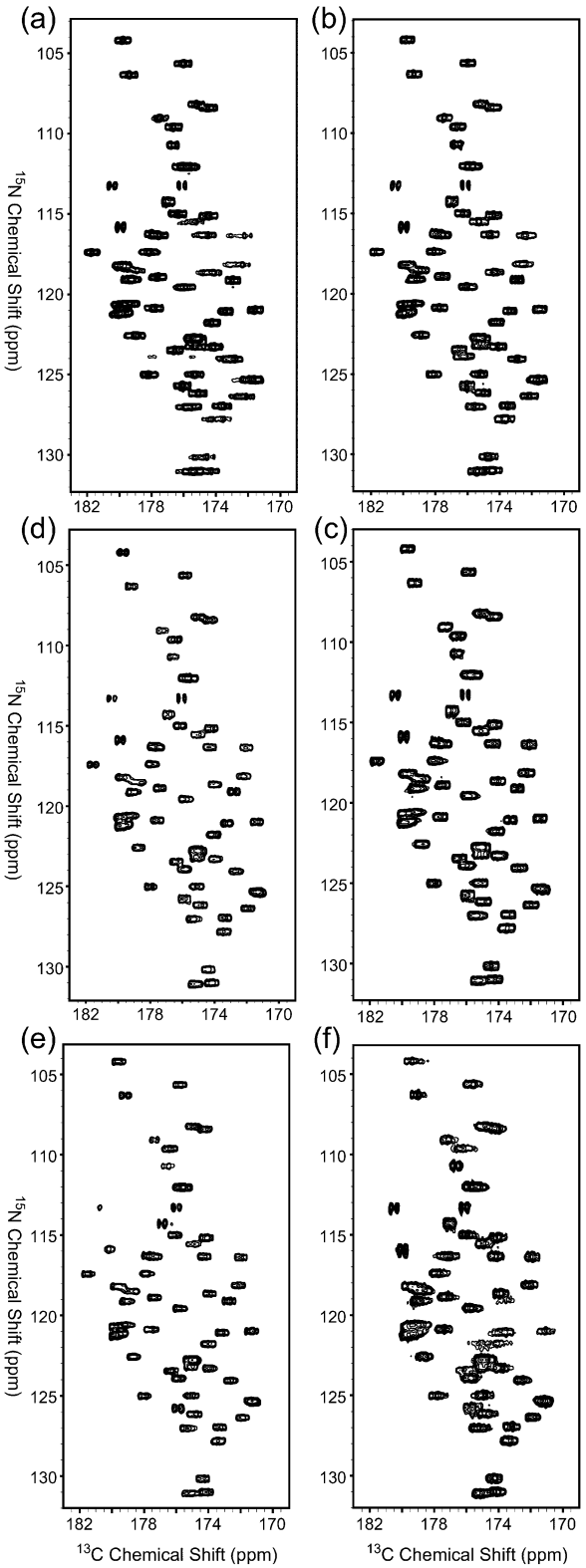

Fig. 1 ^{15}N–^{13}C′ correlation spectra acquired at six different MAS rates with a U–^{15}N,^{13}C labeled sample of GB1 (500 MHz ^{1}H frequency). (a) 8.000 kHz, (b) 9.090 kHz, (c) 10.000 kHz, (d) 11.111 kHz, (e) 12.500 kHz, (f) 13.514 kHz. Spectra were processed without apodization in the directly acquired ^{13}C dimension.

This journal is © the Owner Societies 2008

2D spectra were acquired, with samples prepared identically except for the isotopic labeling pattern; the first sample was U–^{13}C,^{15}N-labeled, the second prepared with 1,3-^{13}C–glycerol as the sole ^{13}C source in the bacterial growth medium, which labels a majority of ^{13}C′ sites but a minimal number of ^{13}C′–^{13}CA pairs.[3] In the U–^{13}C,^{15}N sample, the observed total line widths are typically 0.6 ppm or less, for all sites at least 4 ppm away from R^2 conditions (Fig. 1a–e); the C′ peaks are significantly broader compared to the NC spectra acquired with a sample prepared with 1,3-^{13}C-glycerol as the sole carbon source (Fig. 2). The one-bond $\sim$55 Hz scalar coupling, $^1J_{CC}$, between the C′ and CA sites, accounts for only part of this difference, as examined in more detail below. Spectra were processed in NMRPipe and analyzed in Sparky. Each peak was fit to a linear combination of Gaussians using the integration routine in Sparky, and the peak position was determined as the center of mass (first moment). This procedure was then repeated with the addition of 75 Hz of Gaussian linebroadening. No significant ($>$0.05 ppm) difference in the determined peak positions was observed in the data processed with or without linebroadening.

First we address the dominant effect, that many peak positions change as a function of spinning rate in the U–^{13}C,^{15}N sample, but not in the sparsely labeled sample. This is best appreciated by examining small regions of the NCO spectra of U–^{13}C,^{15}N GB1 at several MAS rates (Fig. 3), which when overlaid illustrate significant shifts in peak position. The effect is as large as 1 ppm for several resonances, including G9C′, G38C′, and A24C′. The same region from the sparsely-^{13}C-labeled sample (narrow, black peaks) shows few MAS rate-dependent changes. (Few significant differences were observed among the spectra acquired with the sparsely labeled sample at six spinning rates. Therefore in Fig. 2 and subsequent, data from the sparsely labeled sample is shown only at 11.111 kHz MAS rate.) Significant effects are observed only among the residue types where the likelihood of encountering directly bonded ^{13}C pairs is high or when an R^2 condition is encountered with another resonance type, such

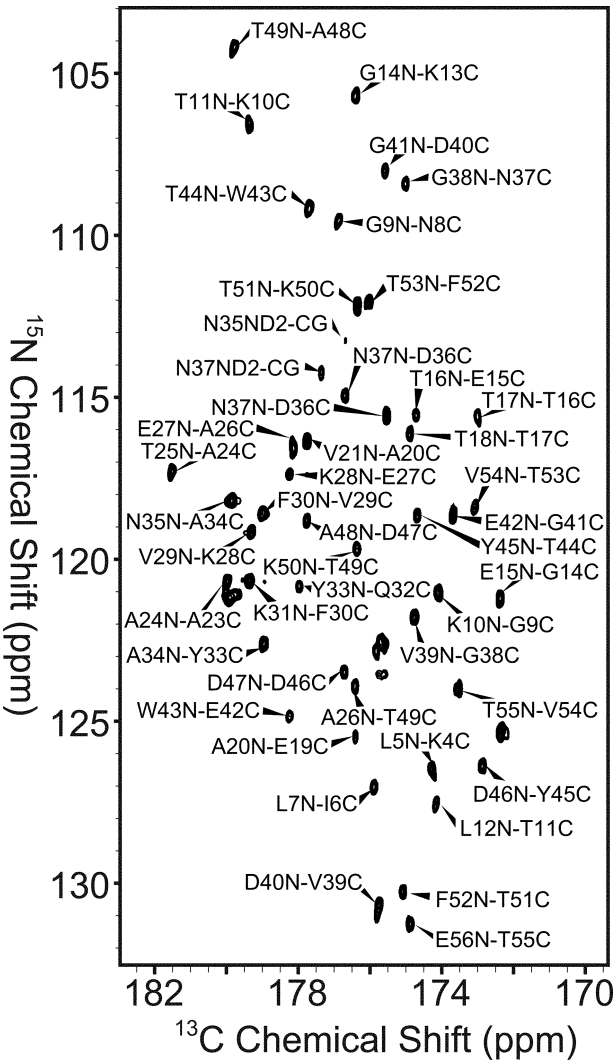

Fig. 2 2D NC spectrum of U–^{15}N GB1 prepared with 1,3-^{13}C-glycerol as the sole carbon source in the bacterial expression medium (500 MHz ^{1}H frequency, 11.111 kHz MAS rate).

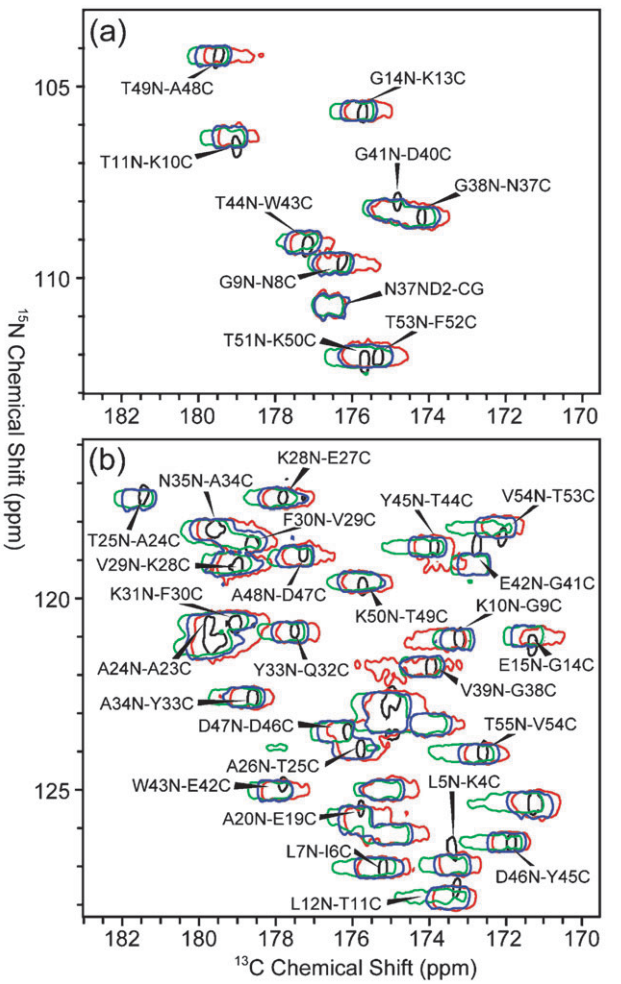

Fig. 3 Overlay of regions of 2D NC spectra for uniformly-^{13}C,^{15}N-labeled GB1 at different MAS rates from Fig. 1 (colored), and the sparsely ^{13}C labeled sample in Fig. 2 (black). The MAS rates illustrated are 8.000 kHz (red), 11.111 kHz (blue), and 13.514 kHz (green).

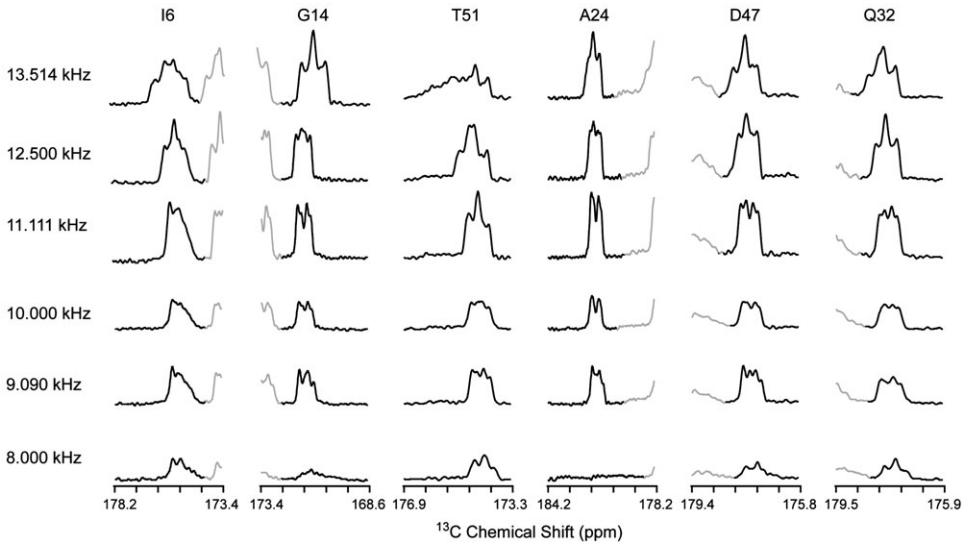

Fig. 4 Lineshapes extracted for several C′ resonances in GB1 as a function of MAS rate. Each slice shows a dramatic range of effects, from dramatic near R^2 broadening (A24, G14 at 8.000 kHz, T51 at 13.514 kHz), to near symmetric doublets (A24 at 10.000, 11.111 kHz, G14 at 11.111 kHz). In most cases a complex powder pattern like lineshape is observed. Neighboring peaks are depicted in grey.

as a CB. This is the case in several of the Thr residues, where R^2 between the C′ and the CB is within 200 Hz of 12.5 kHz. In contrast, essentially all peaks in the U–^{13}C,^{15}N spectra show significant changes over this range of spinning rates, most prominently at ~8 kHz MAS (illustrated in red), which approaches the $n = 2$ R^2 condition for many C′–CA pairs (*i.e.*, the "weak coupling" limit).[23] Here, in addition to an overall broadening, several peaks (*e.g.*, T25N-A24C) are broadened and suppressed in intensity to the noise floor, despite the very high overall sensitivity of the spectra. Fig. 3 shows that all glycine peaks are significantly broadened. Three glycine (G9, G38, and G41) C′ peaks shift by 0.8 to 1.0 ppm relative to the isotropic chemical shift observed in the sparsely labeled sample (Fig. 2). The 13.514 kHz spinning rate (illustrated in green) approaches the other R^2 limit ($n = 1$), especially for threonine residues. T11, T44, and T53 are all significantly broadened, with apparent peak positions shifted by more than 0.5 ppm relative to the 1,3-glycerol–^{13}C-GB1 spectra, and T25 shows an even greater perturbation of 1.6 ppm.

In addition to the changes in peak positions, the sensitivity throughout the spectrum varies substantially as a function of MAS rate. At 8.000 kHz, the average N–CO peak has an SNR of 37 : 1, which improves to 51 : 1 at 9.090 kHz, to 60 : 1 at 10.000 kHz, and reaches a maximum value of 119 : 1 at 11.111 kHz. Further increasing the spinning rate (within the moderate regime) decreases the SNR to 92 : 1 at 12.500 kHz and 59 : 1 at 13.514 kHz, despite the fact that the integrated centerband intensity in the 1D ^{13}C spectra increases with the ratio of MAS rate to CSA magnitude. In all experiments, SPECIFIC ^{15}N–^{13}C cross polarization and TPPM decoupling conditions were both carefully reoptimized at each MAS rate, with typical N–C transfer efficiency of ~60% and nearly identical ^{15}N and aliphatic T_2 relaxation rates. Nonetheless, the degradation of SNR at spinning rates significantly above or below the optimal 11.111 kHz spinning rate was substantial. We therefore attribute this primarily to changes in C′ lineshapes arising from incomplete averaging of the homonuclear ^{13}C–^{13}C dipolar couplings.

These lineshape effects are illustrated in greater detail with slices from several of the resolved cross-peaks in the 2D spectra (Fig. 4). Here all spectra are scaled to identical absolute intensity to demonstrate the large variations in peak height over a range of sites through the protein. The major differences arise from patterns of isotropic chemical shifts and amino acid topology; as such, G14 is representative of the general trend in all glycine residues, and A24 is representative of the alanine residues. In addition, the changes in relative chemical shift of the C′ and CA as a function of secondary structure can further alter the details of the lineshapes. Comparing the absolute peak intensity, the optimal choice of MAS rate within the range studied is 11.111 kHz. This corresponds to the condition that best avoids R^2 conditions for the majority of amino acid residues throughout the protein. Spectra acquired at 8.000 kHz approach R^2 for many residues, especially those with far upfield shifted CA resonances, such as glycine and β-strand conformation alanine residues. Although this MAS limit accelerates polarization transfer along the backbone, a consequence of the same residual homonuclear dipolar coupling, the observed chemical shift spectra are still severely broadened and reduced in signal intensity. At the other extreme, spectra acquired at 13.514 kHz show similar near $n = 1$ R^2 effects for amino acid types with far downfield shifted CA resonances, such as isoleucine (I6) and threonine (*e.g.*, T51). The contribution of the CB resonance, with a chemical shift of ~70 ppm and a ~500 Hz coupling to the C′, likely contributes further to the especially large perturbations in the Thr lineshapes.

2.2 Effect of MAS rate upon apparent isotropic chemical shifts

The chemical shifts as measured directly from spectra of the 1,3-^{13}C–glycerol-labeled sample at several spinning rates are constant within a small experimental error. The standard

 This journal is © the Owner Societies 2008

deviation is ±0.018 ppm and an absolute mean deviation of ±0.042 ppm, primarily due to the Thr peaks observed at 12.500 kHz (as noted above). Because the deviations of the 1,3-^{13}C–glycerol labeled sample are an order of magnitude lower than the shifts measured using the U–^{13}C,^{15}N labeled sample, we assume these peak positions to represent more accurately the actual isotropic chemical shifts. Therefore changes in peak positions as a function of MAS rate in the U–^{13}C,^{15}N sample can be quantified (Fig. 5).

The trends among deviations are similar within a given amino acid type, and so the data are organized in this manner, with site-by-site deviations for glycine (Fig. 5a), alanine (Fig. 5b), threonine (Fig. 5c), aromatic (Fig. 5d) and lysine (Fig. 5e) residues grouped together. These groups represent amino acid types (or highly similar classes) commonly observed in GB1. Consistent with the qualitative trends of the lineshapes reported above, the apparent chemical shifts of glycine residues are significantly perturbed at 8.000 kHz MAS rate, where the C′–CA coupling is within 100 Hz of R^2, whereas spinning rates between 9 and 12 kHz show less than 0.2 ppm deviation. The direction of the shift among glycine residues is not systematic, with G9, G38, and G41 shifting downfield by almost 1 ppm but G14 shifting upfield. This pattern is the result of the G14 having CA resonance downfield of the second-order C′ sideband at 8.000 kHz MAS, while other Gly CA resonances are upfield of their respective C′ second order sidebands.

On the other hand, alanine residues (which are ~300–500 Hz from $n = 2\,R^2$ at 8.000 kHz) show systematic upfield shifts of almost 0.4 ppm; the exception is A24, for which the N–C′ peak at 8.000 kHz is severely depressed in intensity. At all other spinning rates, alanines show a smaller downfield shift of peak position, with the greatest shift for A24 and A26, which are closest to R^2 at 13.514 kHz spinning. Threonine residues (Fig. 4c) show the most complex behavior of all sites considered here, due to the proximity of not only the CA but also the CB to R^2 conditions with C′. MAS rates of 8 to 10 kHz perturb the peak position by less than 0.1 ppm, with greater than 0.5 ppm shifts at 13.514 kHz, except for T49. The T25 linewidth at 13.514 kHz is ~4 ppm broad with two maxima separated by 2.5 ppm, and is excluded from Fig. 5. Aromatic and lysine residues (Fig. 4d and e) show a smaller systematic dependence upon MAS rates within the current range, yet still follow a general trend where at the slowest spinning rate (8.000 kHz), C′ peaks are shifted slightly upfield, and then gradually shift further downfield as the spinning rate is increased, with the 13.514 kHz data showing the largest downfield shifts.

Excluding primary and secondary structural effects, the disparity in observed peak positions relative to accurate chemical shifts derived from the spectra in Fig. 1b, is also informative. Plots of these deviations as a function of residue number are provided in the ESI (Fig. S1).† The poorest agreement is seen at 13.514 kHz, where the average absolute

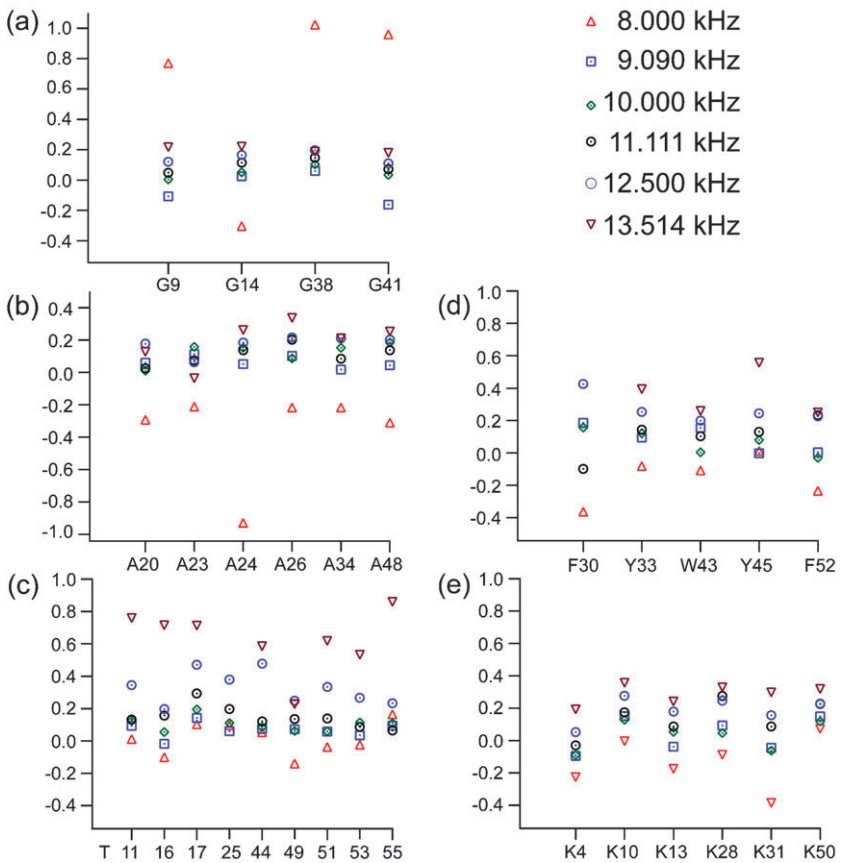

Fig. 5 Deviation of observed isotropic chemical shifts for U–^{13}C sample, compared to shifts obtained from sample prepared with 1,3-^{13}C glycerol. Residue types shown are: (a) glycine, (b) alanine, (c) threonine, (d) aromatic (phenylalanine, tryptophan, and tyrosine), and (e) lysine.

deviation of the measured C′ shift for all sites is 0.36 ppm. The 12.500 kHz data is slightly better, with an average absolute deviation of 0.24 ppm; data at 8.000 kHz MAS also exhibits a prominent (0.2 ppm) deviation. The best agreement is seen for 9.090 kHz MAS (0.09 ppm), followed closely by 10.000 kHz (0.10 ppm) and 11.111 kHz (0.14 ppm). Beyond the mean perturbation, the 8.000 kHz and 13.514 kHz data showed the broadest overall range of perturbation, up to 1.0 ppm relative to the comparable peak from the sparsely labeled sample.

2.3 Quantitative analysis of carbonyl lineshapes

Finally we demonstrate that these lineshape and perturbation effects can be accurately simulated based on previously published models of the spin physics,[24,25,31–38] using a model including Zeeman, isotropic chemical shift, dipolar coupling, scalar coupling and chemical shift anisotropy terms in the Hamiltonian. We assume that TPPM decoupling removes ^{1}H–^{13}C dipolar couplings to first order, resulting in an empirical monoexponential relaxation of transverse ^{13}C coherences. This assumption proves to be reasonable especially for C′ resonances where near-ideal ^{1}H decoupling conditions can be achieved at 500 MHz. Measured T_2 values are greater than 20 ms, corresponding to <16 Hz homogeneous broadening, which is comparable to the chemical shift dispersion in the sample and much less than the $\sim$100 Hz residual dipolar coupling effects observed in many of the spectra. We further assumed that a train of π pulses, one every 8 rotor periods with an *XY-16* phase cycle,[40] decouples the ^{15}N–^{13}C scalar interaction. In addition, MAS averages the truncated heteronuclear dipolar Hamiltonian to this approximation, and the π pulse train further averages the residual heteronuclear coupling. With these assumptions, the Hamiltonian of the system can be simplified as:

$$H = H_{\mathrm{iso}} + H_{\mathrm{CSA}} + H_{\mathrm{D}} + H_J \qquad (1)$$

where H_{iso} represents the isotropic chemical shift for each spin, H_{CSA} is the chemical shift anisotropy, H_{D} is the dipolar coupling between spins, and H_J is the one and two bond J couplings, these are defined explicitly as:

$$\begin{aligned} H_{\mathrm{iso}} &= \omega_{\mathrm{o},I} I_z + \omega_{\mathrm{o,S}} S_z \\ H_{\mathrm{CSA}} &= \omega_{\mathrm{CSA},I}(\alpha_I, \beta_I, \gamma_I) I_z + \omega_{\mathrm{CSA,S}}(\alpha_{\mathrm{S}}, \beta_{\mathrm{S}}, \gamma_{\mathrm{S}}) S_z \\ H_{\mathrm{D}} &= \omega_{\mathrm{D,IS}}(\alpha_{\mathrm{IS}}, \beta_{\mathrm{IS}}, \gamma_{\mathrm{IS}})(3 I_z S_z - I \cdot S) \\ H_J &= \pi J_{\mathrm{IS}} 2 I_z S_z \end{aligned} \qquad (2)$$

Where the I spin is the C′, the S spin is the CA. The angles α, β, γ are the Euler angles which relate each tensor to the common reference frame. Away from R^2, the relative orientation of the CSA tensors to the dipolar axes create asymmetry between the J coupling transitions, where the asymmetry between the two C′–CA J coupling transitions dominate the lineshape. This is the MAS extension of the observations in static spectra which were first reported by Zilm and Grant.[35] We analyzed the data through comparison to a series of simulations in SPINEVOLUTION[41] using this two spin basis. CSA parameters for each ^{13}C site were fixed based on previous studies.[42–44] Following Duma *et al.*,[31] we confirmed this two-spin basis accurately modeled most features of the experimentally measured lineshapes. This assumption was validated by performing 4-spin calculations, including all ^{13}C sites within 2.5 Å of the C′[*i*] (C′[*i*], CA[*i*], CB[*i*], CA[*i*−1]), for a subset of the conditions (ESI, Fig. S3),† which show that 4-spin and 2 spin simulations are essentially indistinguishable in this limit. The possible impact of C′–C′ $n = 0$ R^2 was also considered. In the most extreme case, where the isotropic shifts of the C′–C′ pair were assumed to be identical and the CSA tensors coaxial, a small ($\sim$30 Hz) symmetric splitting was observed, which did not alter the peak position. In more typical scenarios, the splitting was less than 5 Hz.

Following these controls, we then fit a subset of well-resolved C′ sites in the 12.500, 11.111, 10.000, 9.090 and 8.000 kHz spectra to exact simulations. The fitting procedure was facilitated by in-house FORTRAN-77 code that called both external MINUIT minimization libraries,[45] and the SPINEVOLUTION simulation package. In each simulation, the Euler angles of each CSA tensor relative to the common frame were allowed to vary freely using angles reported by Duma, *et al.*[31] as a starting point. The CA isotropic shifts were allowed to vary within a range of 1.5 ppm, and the C′ isotropic shift was allowed to vary over all space. This accounts for referencing imperfections between the experiment and simulation, and to account for the aforementioned uncertainty in the true isotropic chemical shift. As illustrated in Fig. 6, this approach reproduced the dominant features of each site. Further examples of fitted spectra are provided in the ESI (Fig. S2).† Overall, we observed that the best-fit simulations depended most strongly upon the isotropic chemical shift differences, followed by the orientation of the C′ CSA tensor, and the orientation of the CA CSA tensor. Over the four C′ sites illustrated in Fig. 6, there is substantial variation in the resulting lineshape, including large losses in overall peak height and SNR (*e.g.*, for A24 at 8.000 kHz) and doublets with nearly symmetric intensity (A24 and A48 at 11.111 kHz).

As a final test of the validity of this model, a regression analysis was performed in which the best fit for the isotropic shifts from each set of simulated lineshapes was compared with the isotropic shift obtained by direct analysis of experimental spectra acquired with the 1,3-^{13}C–glycerol labeled sample (Fig. 7). We also performed the same analysis for experimental shifts obtained at the other MAS rates. The theoretically fit shifts were in excellent agreement with the 1,3-^{13}C-glycerol data, exhibiting a correlation coefficient, R^2, of 0.9998. The next closest R^2 was for shifts obtained at 11.111 kHz, of 0.9995. Shifts obtained at 8.000 kHz (Fig. 7c) and 13.514 kHz (Fig. 7d) had R^2 values of 0.9978 and 0.9957, respectively, but fairly poor R^2 values of 0.98 and 0.96. All other fits had fit slopes of 1.00 ± 0.01.

3. Experimental

Samples of GB1 were prepared from U–^{15}N,^{13}C GB1 and 1,3-^{13}C-glycerol,^{15}N GB1 was prepared by established methods as discussed elsewhere.[14] In each case, $\sim$18 mg of nanocrystalline material was packed into the central 80% of the sample volume of a limited speed 3.2 mm Varian rotor (Varian, Inc., Fort Collins, Colorado). All experiments were performed using a 500 MHz InfinityPlus spectrometer

 This journal is © the Owner Societies 2008

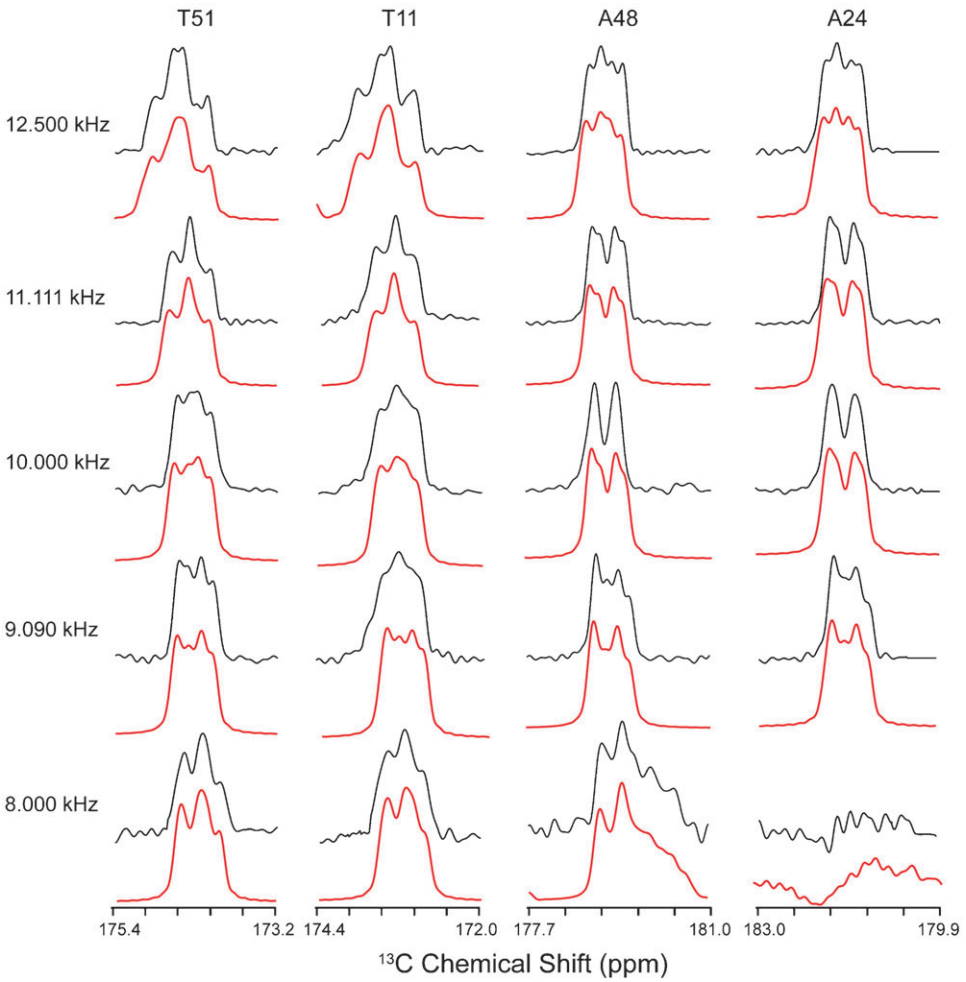

Fig. 6 Experimental lineshapes (black) with best fit simulations (red) for carbonyl resonances in GB1 as various MAS rates as specified.

(Varian, Inc., Palo Alto, California) equipped with a 3.2 mm T3 Balun™ probe specifically optimized for triple resonance ^{1}H–^{13}C–^{15}N experiments. Pulse widths ($\pi/2$) for ^{1}H, ^{13}C, and ^{15}N were 2.1 μs, 2.5 μs, and 5.0 μs, respectively. Spinning was controlled *via* a Varian MAS controller to within ±2 Hz.

Twelve NC′ spectra (six for each sample) were acquired sequentially over a span of two days. The spinning rates employed in this study were 8.000 kHz, 9.090 kHz, 10.000 kHz, 11.111, 12.500 kHz, and 13.514 kHz. In each of these experiments, transverse ^{15}N polarization was generated *via* cross polarization from ^{1}H to ^{15}N (1.4 ms contact time) followed by a ^{15}N acquisition time of 40 ms, transfer of polarization to ^{13}C by SPECIFIC[46] cross polarization, followed by a z-filter and acquisition of the ^{13}C signal. Acquisition time (40 ms in each dimension), sweep width, and the overall duty cycle were kept constant over the course of all experiments. Tangent ramp parameters for the HN cross polarization and SPECIFIC cross polarization were not adjusted from spinning rate to spinning rate, but the center of each ramp was adjusted to satisfy conditions for optimal polarization transfer. A relatively short SPECIFIC contact time of 2 ms was used in all spectra to prevent lineshape analysis from being compromised by ^{15}N–$^{13}C'[i-1]$ peaks appearing near the ^{15}N–$^{13}C'[i]$ peaks. The $\omega_N = 5/2\ \omega_r$, $\omega_C = 7/2\ \omega_r$ SPECIFIC CP condition was maintained at all spinning rates, and decoupling of 85 kHz two pulse phase modulation decoupling (TPPM)[47] was reoptimized precisely (both phase angle and pulse width) at each spinning rate.

4. Conclusion

Several proteins have been fully assigned using SSNMR, using protocols that in general resemble solution NMR but vary in the details.[7] These methods have proved sufficiently general that they are now being applied efficiently in SSNMR to many proteins of unknown structure, where accurate analysis is paramount. Chemical shift assignments provide the basis for additional experimental techniques to measure site-specific distances[48–52] and orientations of molecular fragments to constrain structure.[53–57,42–44] To date the molecules studied, including GB1,[14,53] SH3,[3,13] Crh,[19,58] BPTI,[15] ubiquitin,[9,18] and thiodoxin,[16,17,59] are relatively small proteins, producing spectra in which a relatively small number of peaks are observed, enabling manual confirmation of peak positions in spectra acquired under different conditions of labeling, MAS rate or magnetic field. In larger proteins of unknown structure, such variations in peak positions will present a greater challenge to analyze. Likewise, as observed linewidths improve

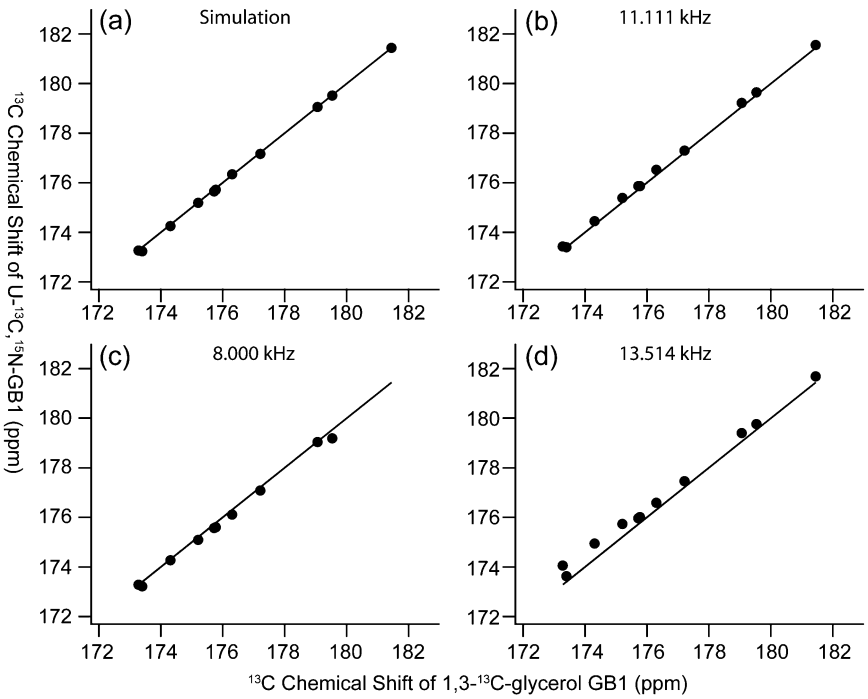

Fig. 7 Plots of determined isotropic chemical shifts for a uniformly-^{13}C,^{15}N-labeled GB1 sample (*y*-axis) in comparison to the sparsely labeled sample (*x* axis). (a) Chemical shifts for the U–^{13}C,^{15}N-sample derived from simulations as described in the text; (b)–(d) chemical shifts derived experimentally from U–^{13}C,^{15}N-labeled GB1 plotted *versus* chemical shifts measured in the 1,3-^{13}C–glycerol labeled sample. The spectra were acquired at (b) 11.111 kHz, (c) 8.000 kHz, and (d) 13.515 kHz MAS rates.

with advances in instrumentation and sample preparation protocols, attention to details of peak position shifts must be systematically understood.

The results presented here illustrate the importance of selection of an appropriate MAS rate to maximize sensitivity and resolution of protein spectra. Care must be exercised in the choice of MAS conditions in order to ensure optimal performance, especially with well-ordered crystalline samples where the inhomogeneous broadening may be a small fraction of a ppm. Even with less well-resolved spectra, the shifts in peak position of $\sim$0.5 ppm could lead to systematic assignment errors in larger proteins, and therefore the effects should be considered when analyzing spectra of multiple protein samples with different isotopic labeling patterns. The most significant adverse consequences of operating away from the optimal condition are assignment errors or missed assignments due to low sensitivity. In addition, inaccurate chemical shifts for carbonyl resonances make it difficult to transfer assignments from one experimental condition (labeling pattern, MAS rate, or magnetic field) to another. For example, chemical shift assignments have so far most often been performed with U–^{13}C,^{15}N labeled samples, and then homonuclear ^{13}C–^{13}C distance estimations obtained with sparsely labeled samples. These samples minimize spin diffusion and relayed transfer effects, and provide maximal resolution and sensitivity for the labeled sites; as examined here, 1,3-^{13}C–glycerol,[3,60] is the most common ^{13}C source used for this purpose, and 2-^{13}C–glycerol[3,9,57,60] provides the complementary labeling patterns, and 1-^{13}C–glucose[57] an even simpler collection of labeled sites. As larger proteins are studied by MAS methods, the challenges associated with transferring chemical shift assignments from one condition to another will be amplified; therefore it is important to consider these effects and, if possible, apply empirical corrections to the data.

In addition, accurately measured isotropic chemical shifts are essential for interpretation of secondary structure on the basis of chemical shifts, using software packages such as TALOS,[66] SHIFTOR,[61] and PREDITOR.[62] These tools are used both to aid in structure determination as well as to validate structural models,[63] for example by comparison to simulated chemical shifts using programs such as SHIFT-X.[64] Along with consistent referencing of SSNMR spectra,[65] knowledge of these effects may help in efforts to combine isotropic and anisotropic chemical shift information for structure determination and refinement.

Acknowledgements

This research was supported by the National Science Foundation (CAREER Award, MCB 0347824). The authors thank the University of Illinois School of Chemical Sciences NMR Facility for technical support, and W. Trent Franks and Professor Eric Oldfield for stimulating discussions regarding chemical shifts.

References

1 A. Watts, I. J. Burnett, C. Glaubitz, G. Grobner, D. A. Middleton, P. J. Spooner, J. A. Watts and P. T. Williamson, *Nat. Prod. Rep.*, 1999, **16**, 419–423.

 This journal is © the Owner Societies 2008

2 G. Grobner, I. J. Burnett, C. Glaubitz, G. Choi, A. J. Mason and A. Watts, *Nature*, 2000, **405**, 810–813.
3 F. Castellani, B. van Rossum, A. Diehl, M. Schubert, K. Rehbein and H. Oschkinat, *Nature*, 2002, **420**, 98–102.
4 A. T. Petkova, Y. Ishii, J. J. Balbach, O. N. Antzutkin, R. D. Leapman, F. Delaglio and R. Tycko, *Proc. Natl. Acad. Sci. U. S. A.*, 2002, **99**, 16742–16747.
5 C. M. Rienstra, L. Tucker-Kellogg, C. P. Jaroniec, M. Hohwy, B. Reif, M. T. McMahon, B. Tidor, T. Lozano-Perez and R. G. Griffin, *Proc. Natl. Acad. Sci. U. S. A.*, 2002, **99**, 10260–10265.
6 C. P. Jaroniec, C. E. MacPhee, V. S. Bajaj, M. T. McMahon, C. M. Dobson and R. G. Griffin, *Proc. Natl. Acad. Sci. U. S. A.*, 2004, **101**, 711–716.
7 A. E. McDermott, *Curr. Opin. Struct. Biol.*, 2004, **14**, 554–561.
8 A. Lange, S. Becker, K. Seidel, K. Giller, O. Pongs and M. Baldus, *Angew. Chem., Int. Ed.*, 2005, **44**, 2089–2092.
9 S. G. Zech, A. J. Wand and A. E. McDermott, *J. Am. Chem. Soc.*, 2005, **127**, 8618–8626.
10 J. L. Lorieau and A. E. McDermott, *J. Am. Chem. Soc.*, 2006, **128**, 11505–11512.
11 A. Cavalli, X. Salvatella, C. M. Dobson and M. Vendrusolo, *Proc. Natl. Acad. Sci. U. S. A.*, 2007, **104**, 9615–9620.
12 C. M. Rienstra, M. Hohwy, M. Hong and R. G. Griffin, *J. Am. Chem. Soc.*, 2000, **122**, 10979–10990.
13 J. Pauli, M. Baldus, B. van Rossum, H. de Groot and H. Oschkinat, *ChemBioChem*, 2001, **2**, 101–110.
14 W. T. Franks, D. H. Zhou, B. J. Wylie, B. G. Money, D. T. Graesser, H. L. Frericks, G. Sahota and C. M. Rienstra, *J. Am. Chem. Soc.*, 2005, **127**, 12291–12305.
15 A. McDermott, T. Polenova, A. Bockmann, K. W. Zilm, E. K. Paulsen, R. W. Martin and G. T. Montelione, *J. Biomol. NMR*, 2000, **16**, 209–219.
16 D. T. Marulanda, M. L. Cataldi, M. Arriaran, V. Polenova and T., *J. Phys. Chem. B*, 2005, **109**, 18135–18145.
17 D. Marulanda, M. L. Tasayco, A. McDermott, M. Cataldi, V. Arriaran and T. Polenova, *J. Am. Chem. Soc.*, 2004, **126**, 16608–16620.
18 T. I. Igumenova, A. J. Wand and A. E. McDermott, *J. Am. Chem. Soc.*, 2004, **126**, 5323–5331.
19 A. Bockmann, A. Lange, A. Galinier, S. Luca, N. Giraud, M. Juy, H. Heise, R. Montserret, F. Penin and M. Baldus, *J. Biomol. NMR*, 2003, **27**, 323–339.
20 F. Castellani, B. J. van Rossum, A. Diehl, K. Rehbein and H. Oschkinat, *Biochemistry*, 2003, **42**, 11476–11483.
21 W. T. Franks, B. J. Wylie, H. L. Frericks, A. J. Nieuwkoop, R. M. Mayrhofer, G. J. Shah, D. T. Graesser and C. M. Rienstra, unpublished results.
22 Y. Li, D. A. Berthold, H. L. Frericks, R. B. Gennis and C. M. Rienstra, *ChemBioChem*, 2007, **8**, 434–442.
23 K. Seidel, A. Lange, S. Becker, C. E. Hughes, H. Heise and M. Baldus, *Phys. Chem. Chem. Phys.*, 2004, **6**, 5090–5093.
24 D. P. Raleigh, M. H. Levitt and R. G. Griffin, *Chem. Phys. Lett.*, 1988, **146**, 71–76.
25 M. H. Levitt, D. P. Raleigh, F. Creuzet and R. G. Griffin, *J. Chem. Phys.*, 1990, **92**, 6347–6364.
26 M. Helmle, Y. K. Lee, P. J. E. Verdegem, X. Feng, T. Karlsson, J. Lugtenburg, H. J. M. de Groot and M. H. Levitt, *J. Magn. Reson.*, 1999, **140**, 379–403.
27 X. Feng, P. J. E. Verdegem, Y. K. Lee, M. Helmle, S. C. Shekar, H. J. M. de Groot, J. Lugtenburg and M. H. Levitt, *Solid State Nucl. Magn. Reson.*, 1999, **14**, 81–90.
28 R. Ramachandran, V. Ladizhansky, V. S. Bajaj and R. G. Griffin, *J. Am. Chem. Soc.*, 2003, **125**, 15623–15629.
29 A. T. Petkova and R. Tycko, *J. Magn. Reson.*, 2004, **168**, 137–146.
30 M. M. Maricq and J. S. Waugh, *J. Chem. Phys.*, 1979, **70**, 3300–3316.
31 L. Duma, S. Hediger, A. Lesage, D. Sakellariou and L. Emsley, *J. Magn. Reson.*, 2003, **162**, 90–101.
32 R. Challoner, T. Nakai and C. A. Mcdowell, *J. Magn. Reson.*, 1991, **94**, 433–438.
33 R. Challoner, T. Nakai and C. A. Mcdowell, *J. Chem. Phys.*, 1991, **94**, 7038–7045.
34 T. Nakai and C. A. Mcdowell, *J. Chem. Phys.*, 1992, **96**, 3452–3466.
35 K. W. Zilm and D. M. Grant, *J. Am. Chem. Soc.*, 1981, **103**, 2913–2922.
36 T. Nakai and C. A. McDowell, *Mol. Phys.*, 1996, **88**, 1263–1275.
37 R. K. Harris, K. J. Packer and A. M. Thayer, *J. Magn. Reson.*, 1985, **62**, 284–297.
38 T. I. Igumenova and A. E. McDermott, *J. Magn. Reson.*, 2003, **164**, 270–285.
39 J. A. Stringer, C. E. Bronnimann, C. G. Mullen, D. H. Zhou, S. A. Stellfox, Y. Li, E. H. Williams and C. M. Rienstra, *J. Magn. Reson.*, 2005, **173**, 40–48.
40 T. Gullion, D. B. Baker and M. S. Conradi, *J. Magn. Reson.*, 1990, **89**, 479–484.
41 M. Veshtort and R. G. Griffin, *J. Magn. Reson.*, 2006, **178**, 248–282.
42 B. J. Wylie, L. J. Sperling, H. L. Frericks, G. J. Shah, W. T. Franks and C. M. Rienstra, *J. Am. Chem. Soc.*, 2007, **129**, 5318–5319.
43 B. J. Wylie, W. T. Franks and C. M. Rienstra, *J. Phys. Chem. B*, 2006, **110**, 10926–10936.
44 B. J. Wylie, W. T. Franks, D. T. Graesser and C. M. Rienstra, *J. Am. Chem. Soc.*, 2005, **127**, 11946–11947.
45 F. James and M. Roos, *Comput. Phys. Commun.*, 1975, **10**, 343–367.
46 M. Baldus, A. T. Petkova, J. H. Herzfeld and R. G. Griffin, *Mol. Phys.*, 1998, **95**, 1197–1207.
47 A. E. Bennett, C. M. Rienstra, M. Auger, K. V. Lakshmi and R. G. Griffin, *J. Chem. Phys.*, 1995, **103**, 6951–6958.
48 A. Hing, S. Vega and J. Schaefer, *J. Magn. Reson.*, 1992, **96**, 205–209.
49 A. W. Hing, S. Vega and J. Schaefer, *J. Magn. Reson., Ser. A* , 1993, **103**, 151–162.
50 C. A. Klug and J. Schaefer, *J. Magn. Reson., Ser. B*, 1996, **110**, 176–181.
51 C. A. Michal and L. W. Jelinski, *J. Am. Chem. Soc.*, 1997, **119**, 9059–9060.
52 C. P. Jaroniec, C. Filip and R. G. Griffin, *J. Am. Chem. Soc.*, 2002, **124**, 10728–10742.
53 W. T. Franks, B. J. Wylie, S. A. Stellfox and C. M. Rienstra, *J. Am. Chem. Soc.*, 2006, **128**, 3154–3155.
54 M. Hong, J. D. Gross and R. G. Griffin, *J. Phys. Chem. B*, 1997, **101**, 5869–5874.
55 M. Hong, J. D. Gross, C. M. Rienstra, R. G. Griffin, K. K. Kumashiro and K. Schmidt-Rohr, *J. Magn. Reson.*, 1997, **129**, 85–92.
56 M. Hong, J. D. Gross, W. Hu and R. G. Griffin, *J. Magn. Reson.*, 1998, **135**, 169–177.
57 M. Hong, *J. Magn. Reson.*, 1999, **139**, 389–401.
58 M. Ernst, A. Detken, A. Bockmann and B. H. Meier, *J. Am. Chem. Soc.*, 2003, **125**, 15807–15810.
59 T. Polenova, M. L. Tasayco, A. McDermott, D. Marulanda, M. Cataldi, V. Arriaran and S. Bai, Experimental NMR Conference, Asilomar, CA, 2004.
60 D. M. LeMaster, *J. Am. Chem. Soc.*, 1996, **118**, 9255–9264.
61 S. Neal, M. Berjanskii, H. Y. Zhang and D. S. Wishart, *Magn. Reson. Chem.*, 2006, **44**, S158–S167.
62 M. V. Berjanskii, S. Neal and D. S. Wishart, *Nucleic Acids Res.*, 2006, **34**, W63–W69.
63 Y. Li, A. Z. Kijac, S. G. Sligar and C. M. Rienstra, *Biophys. J.*, 2006, **91**, 3819–3828.
64 A. Yee, X. Q. Chang, A. Pineda-Lucena, B. Wu, A. Semesi, B. Le, T. Ramelot, G. M. Lee, S. Bhattacharyya, P. Gutierrez, A. Denisov, C. H. Lee, J. R. Cort, G. Kozlov, J. Liao, G. Finak, L. Chen, D. Wishart, W. Lee, L. P. McIntosh, K. Gehring, M. A. Kennedy, A. M. Edwards and C. H. Arrowsmith, *Proc. Natl. Acad. Sci. U. S. A.*, 2002, **99**, 1825–1830.
65 C. R. Morcombe and K. W. Zilm, *J. Magn. Reson.*, 2003, **162**, 479–486.
66 G. Cornilescu, F. Delaglio and A. Bax, *J. Biomol. NMR*, 1999, **13**, 289–302.